IEEE Access
Multidisciplinary | Rapid Review | Open Access Journal

Received July 18, 2017, accepted October 17, 2017, date of publication November 3, 2017,
date of current version December 22, 2017.

Digital Object Identifier 10.1109/ACCESS.2017.2769880

Statistical Analysis of the Influence of Imperfect Texture Shape and Dimensional Uncertainty on Surface Texture Performance

FAN MO[1], CONG SHEN[2], JIA ZHOU[1], AND MICHAEL M. KHONSARI[2]
[1]Department of Industrial Engineering, Chongqing University, Chongqing 400044, China
[2]Department of Mechanical and Industrial Engineering, Louisiana State University, Baton Rouge, LA 70803, USA

Corresponding author: Jia Zhou (zhoujia07@gmail.com)

This work was supported in part by the National Natural Science Foundation of China under Grant 71401018 and Grant 71661167006 and in part by the Chongqing Municipal Natural Science Foundation under Grant cstc2016jcyjA0406.

ABSTRACT This paper investigates the effects of imperfect texture shape and dimensional uncertainty on the surface texture performance (load-carrying capacity and coefficient of friction) by adopting numerical experiments, statistical models, and artificial neural network. The imperfect texture shape is regarded as a polygon, and the uncertain geometrical dimensions include the dimple diameter, the area density, and the dimple depth. Results reveal that the most critical geometric parameters that influence the friction force are manufacturing errors associated with the texture's area density. With respect to the load-carrying capacity and the coefficient of friction, manufacturing errors associated with the dimple diameter are more influential than those of the dimple depth and the area density. It is shown that insofar as the optimization of surface texture performance is concerned, the imperfect texture shape and the dimensional uncertainty associated with the laser texturing with three-sigma performance level are harmless, but manufacturing errors with the one-sigma level can dramatically reduce the load-carrying capacity and increase the coefficient of friction. Specifically, when the dimensions of the area density, the dimple depth, and the dimple diameter are set as 30%, 5.5 μm, and 100 μm, respectively, the imperfect texture shape at the three-sigma level can achieve higher performance than lower levels of control of machining precision.

INDEX TERMS Dimensional uncertainty, imperfect texture shape, parameter optimization, statistical simulation, surface texture performance.

I. INTRODUCTION

Surface texturing and its influence on tribological system performance has been the subject of intensive research in recent years due to its widespread application in mechanical components. Although the performance of textured surfaces is primarily affected by the texture's geometrical parameters, the influence of the ''texture quality'' cannot be neglected. While various fabrication technologies are available to handle the machining requirements of surface texturing, the quality of the individual textures remains to be difficult to regulate. Hence, the actual texture shape and/or the size may deviate from the design value due to the manufacturing errors causing, for example, rough edges around the texture's perimeter due to the limitation of fabrication techniques [1], [2]. As described in what follows, both the imperfect texture shape and the uncertainty on the dimensional accuracy can influence the surface texture performance.

A. SURFACE TEXTURE DIMENSIONS

Numerous studies have focused on the common shapes used for texturing such as circle, hexagon, and square [3]. Studies on other shapes such as spherical, ellipsoidal, circular, elliptical, triangular, and chevron-shaped dimples have also been reported with interesting findings that the ellipsoidal shape and chevron-shape can generate the highest load-carrying capacity among these shapes [4], [5]. By means of adopting model-based virtual texturing and numerical simulations, it has been shown that the texture's bottom shapes involving a micro-wedge and a micro-step bearing tend to yield thicker lubrication films [6]. It has been shown that a shallow depth and a larger diameter dimples tend to yield the larger load-carrying capacity [7].

Another critical parameter is the area density of the dimple for hydrodynamic pressure generation [7]. Theoretical models based on hydrodynamic principles usually

suggest a relatively high area-density to maximize the load-carrying capacity [8]. However, according to the study of Galda *et al.* [9], an area density smaller than 20% is beneficial for lubrication regime transitions. Ibatan *et al.* [10] reviewed several common dimensions of surface texture, including circle, triangle, flat bottom, and curved bottom, and their results show that optimized area density depends on the dimple's shape.

In most previous studies, the effect of each geometric parameter is investigated separately while other parameters are kept constant. However, these parameters are inter-related and the understanding the nature of their collective effects is crucial. A series of experimental tests that use an $L16^{(4\hat{}5)}$ orthogonal array —a black box technique used in statistics testing— are conducted to explore the optimal combination of dimple diameter (50-300 μm), depth (5-20 μm), and area density (5-20%). The results of the study show that with optimum dimple parameters the friction can be reduced up to 77.6% compared to that of untextured surfaces. Specifically, the reported range of the optimum dimple diameter is 100-200 μm, dimple depth is 5-10 μm, and the area density is 5% [11].

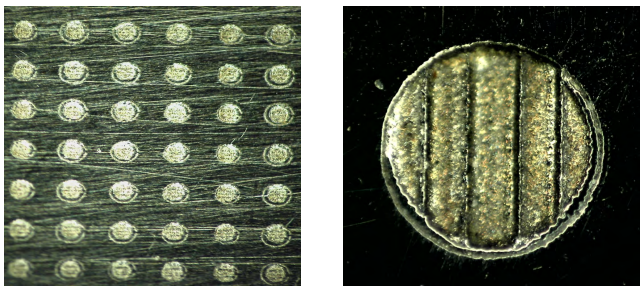

(a) (b)

FIGURE 1. Raised features around the pockets that originates from the ejected molten material. (a) Optical micrograph. (b) Enlarged view of one dimple.

B. IMPERFECT TEXTURE SHAPE AND DIMENSIONAL UNCERTAINTY

Laser surface texturing (LST) is considered to be one of the most effective and efficient methods to generate textures and improve tribological performances. Nevertheless, LST has limitations. The laser ablation mechanism often leads to the formation of raised features around the pockets, which originates from the ejected molten material. Examples from prior research are shown in Fig. 1. The dimple's shape is imperfect, although it is not obvious when the magnification is inadequate. These lateral rims are normally hard due to the microstructural changes caused by the process and can cause severe abrasive wear of the counter surface [1]. To reduce this harmful effect, laser polishing is used to smoothen the roughness of the textured surfaces after the engraving of the surface [2], [12], [13]. For instance, the dimple is first created by a high-fluence laser ablation step and then is smoothed by a low-fluence laser ablation step. The two-step laser surface texturing process can produce dimples with very smooth surfaces, and improved textures quality [14]. The raised features around the pockets also can be found in the topographic image of a spherical dimple (diameter: 1000 μm, depth: 500 μm) in the research reported by Vincent *et al.* [2] and the 2D scanning electron microscope image of a cylindrical dimple (diameter: 100 μm, depth: 4 μm) in research of Amanov *et al.* [15].

The dimensional uncertainty associated with surface textures is another problem inherent to nearly all manufacturing processes. Various statistical methods have been proposed to characterize dimensional uncertainties. Simunovic *et al.* [16] developed a statistical regression model to analysis the influence of face milling cutting parameters on the surface roughness of aluminum alloy. Puh *et al.* [17] applied the Grey-Based Taguchi method to investigate the multi-objective optimization of turning process of an optimal parametric combination to provide the minimum surface roughness. Prasad and Babu [18] utilized the analysis of variance (ANOVA) to evaluate the significance of parameters on overall quality characteristics of the cutting process in an uncertain environment [18].

C. GENERAL RESEARCH QUESTIONS

The existing literature on the analyses of imperfect texture shape and dimensional uncertainty has two drawbacks. First, most of the available studies base their analyses on multiple fixed levels of the uncertainty, or mixed uncertainty from multiple sources, or one-variable-at-a-time technique. These techniques fail to consider the probability of each level and the interaction among variables. Second, of the few available studies that have investigated the influence of imperfect shape, none considered the dimensional uncertainty at the same time. To gain insight into inherent manufacturing errors, both of these effects should be considered simultaneously.

In this study, a general methodology of quantifying uncertainty and imperfect shape from multiple sources is proposed. First, the authors explore the dimensional uncertainty (dimple diameter, area density, and dimple depth) under the condition of imperfect circular shape and then investigate their influence on the surface texture performance (friction force, load-carrying capacity, and coefficient of friction). Second, statistic models are proposed and evaluated, and the key geometric parameter and the optimal performance are identified. The control of machining precision is investigated, and practical implications are proposed.

II. PROBLEM FORMULATION

A. COMPUTATIONAL DOMAIN AND DESIGN VARIABLES

The schematic of a typical textured surface is shown in Fig. 2. The textured surface is stationary during operation, and an upper specimen with a smooth surface is sliding relative to it with a velocity (U), as shown in Fig. 2c. For this given situation, the cavitation pressure, lubricant viscosity, and sliding velocity are fixed. Thermal effects are ignored.

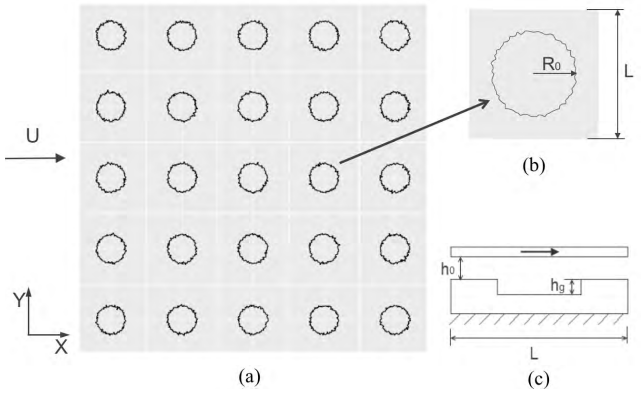

FIGURE 2. Schematic of a textured surface (a) distribution of textures; (b) typical unit cell; (c) side view of a unit cell.

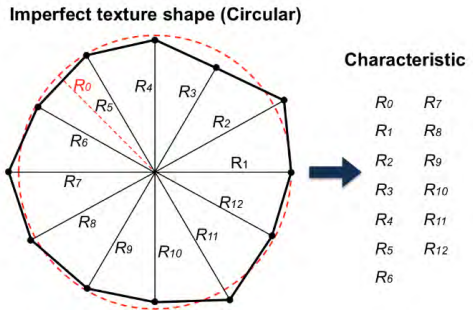

FIGURE 3. Characterization of imperfect texture shape (circular).

The textures are considered as micro dimples uniformly distributed in a square layout on the surface. To simplify the simulation, a single unit cell is used as the computational domain.

The dimple border is rough because of the uncertainly manufacturing process, and the texture shape is considered as imperfect circle (as shown in Fig. 2b). Prediction with the present model is undertaken by dividing the texture into 12 sections evenly distributed in the circumferential direction with a spacing of 30 degrees (as shown in Fig. 3). Therefore, the design variables for a texture shape are the radii (R_1, R_2, R_3, ..., and R_{12}); the diameters (d_1, d_2, d_3, ..., and d_{12}) are corresponding to these radii. Three performance parameters—friction force, load-carrying capacity, and coefficient of friction— on single unit cell are investigated at the same time. The optimal performance corresponds to minimum values of the friction force and the coefficient of friction, and the maximum value of the load-carrying capacity.

The film thickness equation has two regions, one within the groove and the other outside the groove. Periodic boundary conditions are applied in the sliding direction (X), and the boundaries in the other direction (Y) are kept at ambient pressure. Surfaces are assumed to be rigid, and the density (ρ) and viscosity (μ) variations across the thin lubricant are negligible. Under the typical thin-film lubrication assumptions, the equation governing the hydrodynamic pressure distribution is the Reynolds equation. The half-Sommerfeld cavitation boundary condition is applied in this study. In accordance with prior research [19], [20], the Reynolds equation can be solved based on the given film profile and boundary conditions, and the friction force (F) and the load-carrying capacity (W) are non-dimensionalized by:

$$\bar{F} = \frac{F}{P_a S} = \frac{8F}{\left(\sum_{i=1}^{n}(d_i d_{i+1}) + d_1 d_n\right) sin\frac{2\pi}{n} P_a}, \quad (n = 12)$$
$$\bar{W} = \frac{W}{P_a S} = \frac{8W}{\left(\sum_{i=1}^{n}(d_i d_{i+1}) + d_1 d_n\right) sin\frac{2\pi}{n} P_a}, \quad (n = 12) \tag{1}$$

where $\bar{F}$ and $\bar{W}$ are the dimensionless friction force and load-carrying capacity, P_a is the ambient pressure in the simulation, and S is the area of the imperfect texture shape.

B. STATISTICAL PARAMETERS

In order to statistically interpret the texture dimensions and corresponding performance, the parameter definitions are introduced as follows:

x_1	$\cong$ dimple diameter, d_0
x_{d1}, x_{d2}, x_{d3}, ..., and x_{d12}	$\cong$ dimple diameters, d_1, d_2, d_3, ..., and d_{12}, respectively
$d_{(mean)}$	$\cong$ average value of d_1, d_2, d_3, ..., and d_{12}
$d_{(sd)}$	$\cong$ standard deviation of d_1, d_2, d_3, ..., and d_{12}
x_2	$\cong$ area density, S_p
x_3	$\cong$ dimple depth, h_g
e_{d1}, e_{d2}, e_{d3},..., and e_{d12}	$\cong$ manufacturing errors of X_{d1}, X_{d2}, X_{d3}, ..., and X_{d12}, respectively
$e_{d(mean)}$	$\cong$ average value of e_{d1}, e_{d2}, e_{d3}, ..., and e_{d12}
$e_{d(sd)}$	$\cong$ standard deviation of e_{d1}, e_{d2}, e_{d3}, ..., and e_{d12}
e_2	$\cong$ manufacturing errors of X_2
e_3	$\cong$ manufacturing errors of X_3
y_1	$\cong$ friction force, F
y_2	$\cong$ load-carrying capacity, W
y_3	$\cong$ coefficient of friction, f
Δy_1	$\cong$ variation of F
Δy_2	$\cong$ variation of W
Δy_3	$\cong$ variation of f
x_{RE}	$\cong$ roundness error of the texture shape
x_{RSE}	$\cong$ roundness standard error of the texture shape

Roundness error is usually calculated using the least square method which gives a least square circle (LSC) by separating the sum of total areas of the inside and outside it in equal amounts. Roundness error is the difference value between the maximum and minimum distance from this LSC. Since the manufacturing errors of diameters obey normal

distribution, LSC is evaluated by the basic circle from design in this research, and roundness error of the imperfect circle is estimated by following equation.

$$x_{RE} = \max\{(d_1 - d_0), (d_2 - d_0), \ldots, (d_{12} - d_0)\} - \min\{(d_1 - d_0), (d_2 - d_0), \ldots, (d_{12} - d_0)\} \quad (2)$$

Roundness error only captures the extreme value of circumference's variation and it is likely to lose some information. To measure the variation more comprehensively, standard errors between the real values of diameters and the design values are calculated using following equation.

$$x_{RSE} = \sum_{i=1}^{12} (d_i - d_0)^2 \quad (3)$$

It is shown that $e_{d(sd)}$ is identical with x_{RSE}. Therefore, $e_{d(mean)}$ can be used to measure the manufacturing error of the dimple diameter, and $e_{d(sd)}$ and x_{RE} can be used to measure the influence of imperfect texture shape.

It follows, therefore, that the goal of the research is to investigate how the texture dimensions (i.e., x_{d1}, x_{d2}, x_{d3}, . . ., x_{d12}, x_2, and x_3) and their associated manufacturing errors (i.e., e_{d1}, e_{d2}, e_{d3}, . . ., e_{d12}, e_2, and e_3) influence the dependent variables (i.e., Δy_1, Δy_2, and Δy_3) and to further reflect the influence through statistic models. In the analyses that follows, the working conditions are fixed. Minimum film thickness (h_0) is 5 μm, lubricant viscosity (μ) is 0.38 Pa · s, sliding velocity (U) is 1 m/s, and ambient pressure (P_a) and cavitation pressure (P_c) are 100 kPa. The range for textured geometry in the simulations is 100-2000 μm for the dimple diameter, 5-30% for the area density, and 1-10 μm for the dimple depth.

C. ASSUMPTIONS

There are three assumptions in accordance to the previously reported research [19]. First, the three geometrical parameters (dimple diameter, area density, and dimple depth) follow uniform distribution, and their manufacturing errors follow normal distribution, since geometrical parameters are usually determined by the designers, and manufacturing errors are random in manufacturing processes. Second, the laser texturing reaches the three-sigma performance level since the three-sigma level is a common quality metric in manufacturing and is widely used to set the control limit. Third, the relative tolerance band of $e_{d(mean)}$ is ± 10 μm, which differs from prior research. The relative tolerance band of e_2 and e_3 is $\pm 1\%$, and all the manufacturing errors are independent. The tolerance band of $e_{d(mean)}$ is set as ± 10 μm according to the characteristics of the manufacturing method that the diameter errors caused by laser texturing is likely to be a constant value because that it results from location errors. The tolerance band of e_2 and e_3 is set to be relative (e_2 is $\pm 1\%$ and e_3 is $\pm 1\%$). Those larger than 1% of the designed size or smaller than 1% of the designed size are considered to be defective. That is, e_2 and e_3 within the range from 99% to 101% of the average.

D. STATISTICAL MODELS AND NUMERICAL EXPERIMENT

To give a general overview of the relationship between the texture performance and texture dimensions, regression models that do not include the variables of manufacturing errors are first explored. Linear models, quadratic models, cubic models, logarithmic models, and logarithmic cubic models are examined. The data that are used to estimate the parameters in regression models are generated by numerical experiment that solve the Reynolds equation to generate data of texture dimensions and associated manufacturing errors. R programs and Matlab®programs are used to numerically generate the necessary data, conduct the numerical experiment, and build the statistical models. Finally, according to the fitting results of models, the authors further add the manufacturing errors of texture dimensions into the models that have high validity. The numerical experiment and the statistical models are adopted from prior research [19]. In view of the large number of variables and the complex relationship between them, the traditional linear and nonlinear statistical models may be difficult to fit the data well. Back-propagation (BP) neural network, a machine learning method to fit and predict data with high accuracy, is used for this purpose. It is self-adaptive in a way that simulative neurons in the network organize themselves continuously according to the feedback of the output and the whole network. Monolayer BP neural network is adopted after building traditional statistical models.

III. RESULTS OF STATISTICAL MODELS

A. MODEL WITH SINGLE FACTOR

The numerical experiments data are analyzed in three steps. The first section assumes that performance of surface textures is only influenced by a single factor at a time, and the interaction between any two factors is neglected. The next section assumes that performance of surface textures is influenced by all factors, and their interactions are considered. Third, monolayer BP neural network with different parameters is tested, and one suitable model is adopted for prediction.

Each manufacturing error (i.e., e_{d1}, e_{d2}, e_{d3}, . . ., e_{d12}, e_2, and e_3) is divided into 3 levels (negative, neutral, and positive) by quartiles. The data from numerical experiment is preliminarily analyzed through multivariate analysis of variance (MANOVA). As shown in Table 1, all manufacturing errors significantly influence the load-carrying capacity and the friction coefficient. However, only S_p and its manufacturing error have significant influence on the friction force. All manufacturing errors of d_1, d_2, d_3, . . ., and d_{12} affect the surface texture performance in the same way and have equivalent influence on all performance dimensions since they are generated by the same mechanism. Therefore, $e_{d(mean)}$ is used to measure the general influence of manufacturing errors of the dimple diameters (e_{d1}, e_{d2}, e_{d3}, . . ., and e_{d12}).

Fig. 4 shows the influence of the manufacturing errors due to texture dimensions on the average variations of the friction force, the load-carrying capacity, and the

TABLE 1. The statistical parameters from MANOVA about texture dimensions and associated manufacturing errors on texture performance.

	Δy_1			Δy_2			Δy_3		
	df[a]	*F-value*[b]	*p-value*[c]	*df*	*F-value*	*p-value*	*df*	*F-value*	*p-value*
$e_{d(mean)}$	2	0.029	0.972	2	48.180	<0.001*	2	131.783	<0.001*
e_2	2	1357.500	<0.001*	2	216.921	<0.001*	2	4.677	0.009*
e_3	2	0.290	0.749	2	71.557	<0.001*	2	39.229	<0.001*
$e_{d(mean)} \times e_2$	4	0.015	1.000	4	4.957	<0.001*	4	0.960	0.428
$e_{d(mean)} \times e_3$	4	0.000	1.000	4	1.259	0.284	4	3.319	0.010*
$e_2 \times e_3$	4	0.009	1.000	4	0.931	0.445	4	0.029	0.998
d_0	1	0.573	0.449	1	25.418	<0.001*	1	184.246	<0.001*
S_p	1	4.240	0.040*	1	46.447	<0.001*	1	288.762	<0.001*
h_g	1	0.086	0.769	1	0.390	0.532	1	94.712	<0.001*

[a]*df* = degrees of freedom, which refers to the number of values in the final calculation of a statistic that is free to vary.
[b]*F-value* is referred to as the F statistic.
[c]*p-value* is defined as the probability of obtaining a result equal to or "more extreme" than what is actually observed, when the null hypothesis is true.
*Significant at 0.05 level (two-tailed).

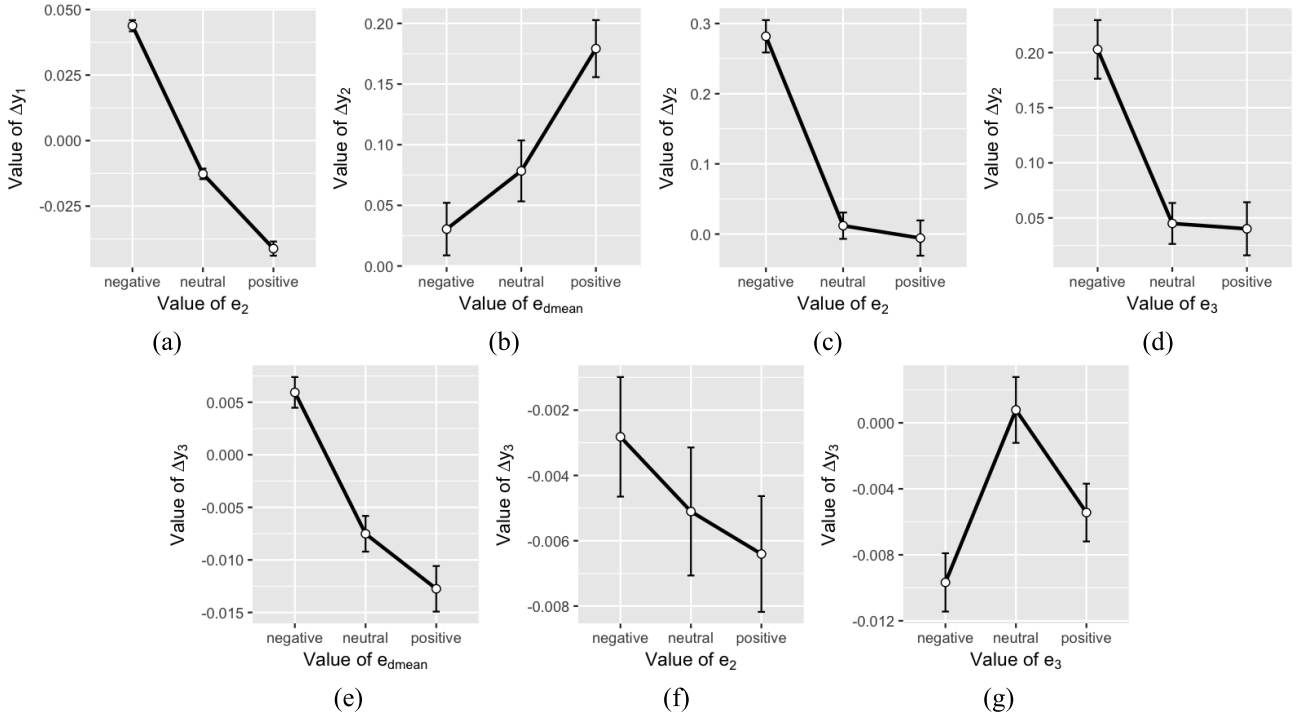

FIGURE 4. The influence of manufacturing errors on (a) variations of the friction force (Δy_1), (b), (c), and (d) variations of the load-carrying capacity (Δy_2), and (e), (f), and (g) variations of the friction coefficient (Δy_3).

friction coefficient. Δy_1 is only significantly affected by e_2, and it decreases as e_2 is increased (as shown in Fig. 4a). As shown in Fig. 4b, 4c, and 4d, Δy_2 is significantly affected by all manufacturing errors.

No matter which direction of the variations of $e_{d(mean)}$, e_2, and e_3 (i.e., negative, neutral, or positive), the mean value of Δy_2 is nearly positive. The performance of load-carrying capacity is increased when manufacturing errors occur. Differences of performance between different levels of e_2 are obvious. However, it is not clear whether the change of the performance caused by manufacturing errors is significant, and this is further elaborated in the section entitled "Discussion". Furthermore, variations around the negative valu e of e_2 and e_3 result in higher load-carrying capacity compared with neutral variations and positive variations. As to Δy_3, it is nearly generally negative no matter the value of the variations of $e_{d(mean)}$, e_2, and e_3 (as shown in Fig. 4e, 4f, and 4g). There is negative correlation between Δy_3 and $e_{d(mean)}/e_2$, which reveals that the friction coefficient is lower when the $e_{d(mean)}$ and e_2 are higher.

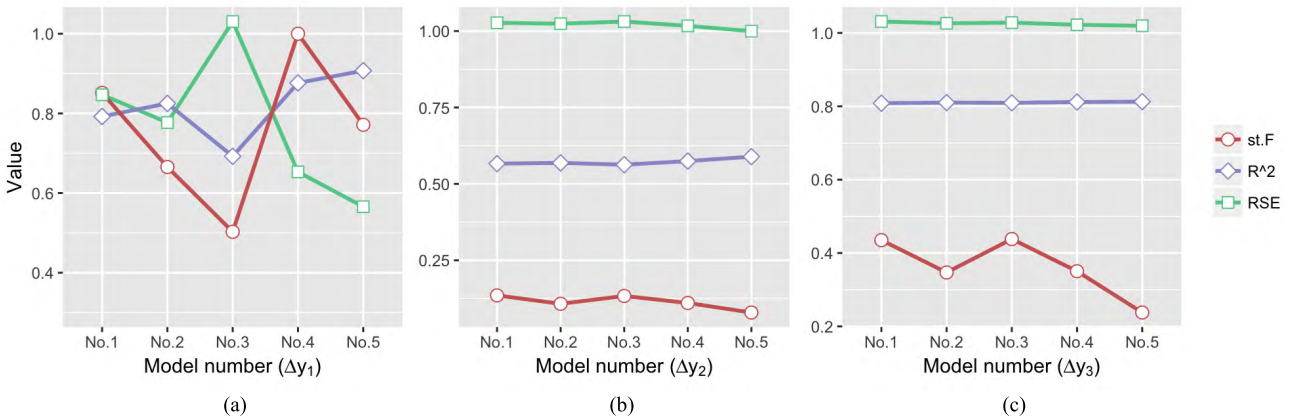

FIGURE 5. Statistical parameters of *st.F*, R^2, and *RSE* in models of (a) Δy_1, (b) Δy_2, and (c) Δy_3 (R^2 = Adjusted R-Squared, which is a modified version of R-squared that has been adjusted for the number of predictors in the model. R-squared refers to how close the data are to the fitted regression line. The large R^2, the better is the result. *RSE* = Residual Standard Error, which is an estimate of this standard deviation, and substantially expresses the variability in the dependent variable "unexplained" by the model. The small *RSE*, the better is the result).

B. MODELS WITH MULTIPLE FACTORS AND INTERACTIONS

The influence of all factors and their interactions are considered in this section. The detailed procedure to derive models is mentioned in above section. Five models with multiple factors are proposed, and these models have comparative power to explain dependent variables. To explore the most appropriate models, statistical parameters of *st.F* (standardized F-value), R^2, and *RSE* are compared (as shown in Fig. 5). With a large value of *st.F* and R^2 and a small value of *RSE*, the models become more powerful. In order to reduce the complexity and build a simple and comprehensible model, the cubic model (i.e., the model No.2 in Fig. 5) is chosen for fitting Δy_1, and the quadratic model (i.e., the model No.1 in Fig. 5) is chosen for fitting Δy_2 and Δy_3.

Above models which include manufacturing errors of d_1, d_2, d_3, ..., and d_{12} have equivalent impact on the performance for the reason of predicting Δy_1, Δy_2, and Δy_3 more accurately and completely. In order to improve models' effectiveness and efficiency, the number of their independent variables should be reduced, so d_1, d_2, d_3, ..., and d_{12} are described by $d_{(mean)}$ and $d_{(sd)}$. In addition, the models of y_1, y_2, and y_3 are analyzed for purpose of comparing the difference between them and the models based on their variations.

As given in Table 2, models of y_1, y_2, and y_3 have better performance than models of Δy_1, Δy_2, and Δy_3. However, the predictions of Δy_1, Δy_2, and Δy_3 conform with the aims of this research better; models of Δy_1, Δy_2, and Δy_3 are more suitable for measuring the variations. The equations of these final models are described as follows:

The friction force:

$$\begin{aligned}\ln(|\Delta y_1|) = &-1.4456 - 41.0295 \times S_p + 1.2441 \times 10^3 \times e_2 \\ &+ 70.6939 \times S_p \times S_p + 6.8074 \times 10^6 \times e_2 \times e_2 \\ &- 1.4691 \times 10^4 \times S_p \times e_2 \\ &+ 6.6636 \times 10^5 \times S_p \times h_g \end{aligned}$$

TABLE 2. Models of different expressions of variables.

Independent Variable	Dependent Variable	*F-value*	R^a	*RSE*
d_1, d_2, d_3, ..., and d_{12}	Δy_1	838.96	82.51%	0.7771
	Δy_2	170.35	56.62%	1.0271
	Δy_3	548.55	80.84%	1.0311
d_1, d_2, d_3, ..., and d_{12}	y_1	19936554.69	99.99%	0.0023
	y_2	968780.77	99.99%	0.0163
	y_3	667569.59	99.98%	0.0186
$d_{(mean)}$ and $d_{(sd)}$	Δy_1	838.96	82.51%	0.7771
	Δy_2	195.67	53.57%	1.0626
	Δy_3	676.14	80.01%	1.0533
$d_{(mean)}$ and $d_{(sd)}$	y_1	19936554.69	99.99%	0.0023
	y_2	1142995.87	99.99%	0.0172
	y_3	804825.40	99.98%	0.0193

$$\begin{aligned}&+ 2.4173 \times 10^9 \times e_2 \times e_2 \times e_2 \\ &- 7.3389 \times 10^7 \times S_p \times S_p \times e_2 \times e_2 \\ &- 1.4164 \times 10^{11} \times S_p \times S_p \times h_g \times h_g \\ &- 5.2914 \times 10^{19} \times e_2 \times e_2 \times e_3 \times e_3 \end{aligned} \quad (4)$$

The load-carrying capacity:

$$\begin{aligned}\ln(|\Delta y_2|) = &-4.0711 + 2.3083 \times 10^3 \times d_0 - 8.8529 \times S_p \\ &+ 2.8337 \times 10^5 \times h_g \\ &+ 2.5964 \times 10^5 \times e_{d(mean)} \\ &+ 3.1724 \times 10^5 \times d_0 \times d_0 \\ &- 2.4387 \times 10^{10} \times h_g \times h_g \\ &+ 3.7820 \times 10^{10} \times e_{d(mean)} \times e_{d(mean)} \\ &+ 2.2778 \times 10^{10} \times e_{d(sd)} \times e_{d(sd)} \end{aligned}$$

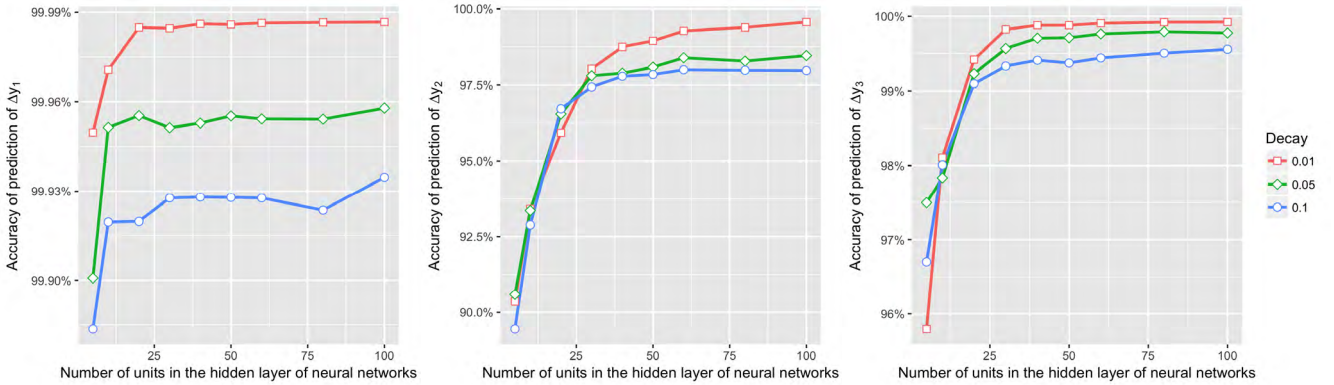

FIGURE 6. Accuracy of the models that built based on BP neural network with different parameters.

$$
\begin{aligned}
&+1.5692\times10^{5}\times e_2\times e_2\\
&-2.4202\times10^{8}\times d_0\times e_{d(mean)}\\
&-3.3317\times10^{8}\times d_0\times e_{d(sd)}\\
&-1.7203\times10^{3}\times S_p\times e_2\\
&+3.9812\times10^{9}\times e_2\times e_3
\end{aligned}
\tag{5}
$$

The coefficient of friction:

$$
\begin{aligned}
\ln(|\Delta y_3|) = &-4.2506-5.9680\times10^{3}\times d_0+13.1233\times S_p\\
&-2.6087\times10^{5}\times h_g\\
&+2.8389\times10^{5}\times e_{d(mean)}\\
&+1.7777\times10^{5}\times e_{d(sd)}+4.6704\times10^{2}\times e_2\\
&+2.3152\times10^{6}\times d_0\times d_0-43.1271\times S_p\times S_p\\
&+2.3073\times10^{10}\times h_g\times h_g\\
&+4.2851\times10^{10}\times e_{d(mean)}\times e_{d(mean)}\\
&-1.6718\times10^{5}\times e_2\times e_2\\
&+1.1361\times10^{14}\times e_3\times e_3\\
&-2.6713\times10^{8}\times d_0\times e_{d(mean)}\\
&-2.1064\times10^{8}\times d_0\times e_{d(sd)}\\
&-1.0300\times10^{3}\times S_p\times e_2\\
&-2.5485\times10^{9}\times e_2\times e_3
\end{aligned}
\tag{6}
$$

The models can explain above 82.51%, 53.57%, and 80.01% of variance independent variables for the friction force, the load-carrying capacity, and the friction coefficient, respectively.

C. MODELS WITH MONOLAYER BP NEURAL NETWORK

BP neural network is used to fit the data for improving the accuracy of models. The approach of machine learning has high goodness of fit but may cost more operation time and result in the overfitting problem. To choose the appropriate models, models' parameters are tested. The number of units in the hidden layer of neural networks is set from 5 to 100, and the parameter for weight decay is set as 0.01, 0.05, and 0.1. The data from numerical experiment are split into training data set (70%) and validation data set (30%) by random sampling method. The accuracy of prediction of the training data is shown in Fig. 6.

In general, models' accuracy improved as the decay decreased and the size of hidden layer increased. The models are stable when the size of hidden layer is up to about 50. Therefore, the decay is set as 0.01 and the size of hidden layer is set as 60 in the models with back-propagation neural network.

The goodness of fit of those models is 99.99% for Δy_1, 99.27% for Δy_2, and 99.91% for Δy_3 in terms of training data. In validation data, the goodness of fit is 99.73% for Δy_1, 97.51% for Δy_2, and 96.52% for Δy_3. The accuracy is decrease due to the overfitting problem, but it is still higher than 96.50%, which is acceptable. The real value and predicted value in the whole dataset are very close, as shown in Fig. 7.

IV. DISCUSSION

A. CRITICAL TEXTURE DIMENSIONS

In these models, the T value of each independent variable is attained. It represents the influence degree of each independent variable on the friction force, the load-carrying capacity, and the coefficient of friction. The roundness error of texture shape is considered, and these models are rerun. Based on the T value, the importance of each independent variable can be visualized in Fig. 8.

A number of factors have significant influence on the variations of the friction force, the load-carrying capacity, and the friction coefficient. For the friction force, the most influential factor is manufacturing errors of area density. For the load-carrying capacity, the most influential factors are manufacturing errors of dimple diameter, and the shape (represented by $e_{d(sd)}$ and roundness). For the friction coefficient, the manufacturing errors of dimple diameter are more influential than that of the dimple depth and the area density. The imperfect shape has a lower level of impact compared with manufacturing errors of dimple diameter but has the similar impact with the manufacturing errors of area density.

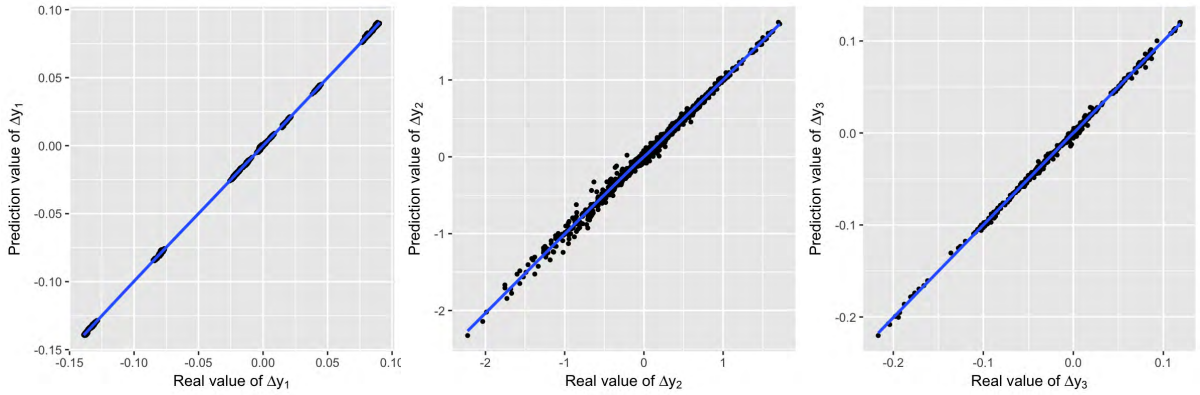

FIGURE 7. The actual value and the predicted value for each performance parameter.

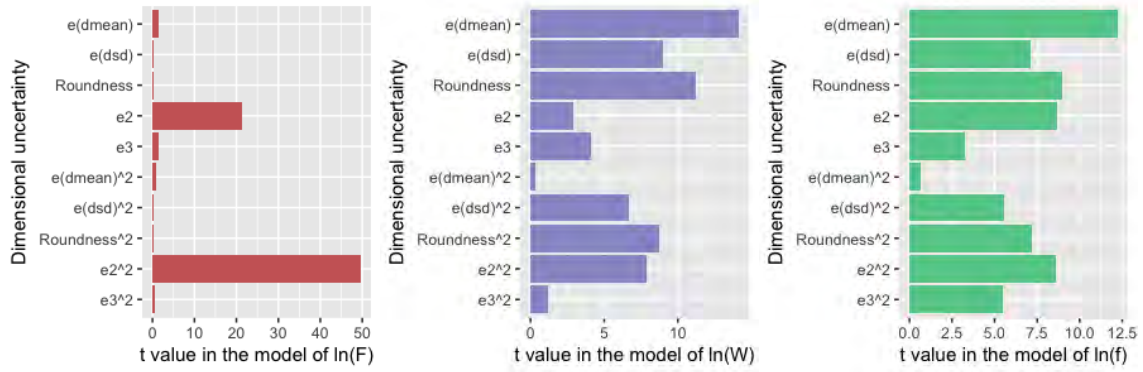

FIGURE 8. The importance of each independent variable in the cubic model.

B. VARIATIONS OF SURFACE TEXTURE PERFORMANCE

The manufacturing errors have greater influence in models of Δy_1, Δy_2, and Δy_3 compared with models of y_1, y_2, and y_3. One explanation is that Δy_1, Δy_2, and Δy_3 directly represent the influence of manufacturing errors on variations of surface texture performance. However, it is not clear whether Δy_1, Δy_2, and Δy_3 are obvious based on y_1, y_2, and y_3, so rates of them are calculated and are shown in Fig. 9.

Generally, the variation of the friction force is less than that of the load-carrying capacity and the friction coefficient, which means that the dimensional uncertainty and imperfect texture shape only have little influence on friction force. As to the load-carrying capacity and the friction coefficient, range of variations is from -8% to 8%, and there are a large number of outliers. About two fourths of the rates are in the range of 0% to 1% (for $\Delta y_2/y_2$) or -1% to 0% (for $\Delta y_3/y_3$). The manufacturing errors lead to the increase in the load-carrying capacity and the decrease in the friction coefficient about 0.3% and 0.6% on average. The manufacturing errors slightly, but insignificantly, improve the performance of surface textures.

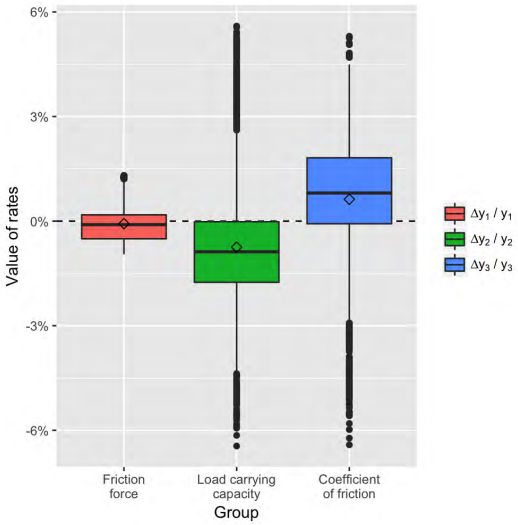

FIGURE 9. Boxplot of rates of Δy_1, Δy_2, and Δy_3 and y_1, y_2, and y_3.

C. OPTIMAL PERFORMANCE

The analysis of critical texture dimensions reveals that manufacturing errors usually improve the surface texture performance at the three-sigma level. Therefore, in order to obtain the optimum texture performance, the variations of the friction force and the friction coefficient that caused by manufacturing errors should be controlled as negative values, and those of the load-carrying capacity should be controlled

TABLE 3. Optimized values and corresponding parameters.

		Δy_1	Δy_2	Δy_3
Optimal value of performance		-0.2357 (min)	4.5217 (max)	-0.3056 (min)
Corresponding values of manufacturing errors of texture dimensions	$e_{d(mean)}$ (-20-20 μm)	(-20)*	20	2.9
	$e_{d(\mathrm{sd})}$ (0-10)	(1.5)*	6.3	8.2
	Roundness (0-20)	(20)*	8.5	15
	e_2 (-0.081-0.081%)	0.081	-0.081	-0.081
	e_3 (-0.021-0.021 μm)	0.021	-0.021	0.020

Note: the range of $e_{d(mean)}$, roundness, e_2, and e_3 is calculated by the tolerance band of d_0, S_p, and h_g. The range of $e_{d(\mathrm{sd})}$ is determined by the range of $e_{d(\mathrm{sd})}$ value in the numerical experiment. Besides, although there are internal relations among $e_{d(mean)}$, $e_{d(\mathrm{sd})}$, and roundness, the models consider them as independent variables.
*The variables do not have significant influence on this performance dimension according to the results from Fig. 8, so they are ignorable.

as large positive values. A generalized simulated annealing algorithm, from "GenSA" package in R [21], is used to calculate the minimum value of Δy_1, Δy_2, and Δy_3. The results are shown in Table 3.

Regarding the manufacturing errors of texture dimensions, Δy_2 calls for a large value of $e_{d(mean)}$ and a moderate value of $e_{d(\mathrm{sd})}$ and roundness. This means that the dimple shape should be controlled as a rough circle, and size of the circle is likely to be manufactured as large as possible. The result is consistent to the demand of the maximum value of d_0 [19]. As to Δy_3, it requires a moderate value of $e_{d(mean)}$. The optimal values of $e_{d(\mathrm{sd})}$ and roundness are large, so the dimple shape should also be imperfect. Besides, it is found that Δy_2 and Δy_3 call for minimum value of e_2. It should be emphasized that the predictions, which adopt the hybrid method of BP neural network and genetic algorithm, are good at predicting optimal values of dependent variables (i.e., surface performance) instead of independent variables (i.e., the shape of textures). The reason is that a subtle change in nerve cells would result in great variation in the whole BP neutral network because of back-adjusting. Therefore, stable results are given after making multiple runs of the programs, and only the same trends of optimal parameters are discussed.

In a prior research [19], a large dimple diameter (around 1883 μm) and a moderate dimple depth (5.5-6.5 μm) was set in order to obtain high performance in terms of load-carrying capacity and friction coefficient. Since the texture dimensions have the main influence on texture performance and their manufacturing errors only have limited influence, the optimized texture dimensions in reference [19] are recommended. Then, the corresponding values the textures' manufacturing errors are given in Table 3.

TABLE 4. Differences between $y1, y2, y3$ with manufacturing errors and $y1, y2, y3$ without manufacturing errors.

	Comparisons	*T-value* [a]	*df*	*p-value*
Manufacturing errors at the three-sigma level	y_1 with e VS y_1 without e	0.025	6748	0.9804
	y_2 with e VS y_2 without e	0.108	6748	0.9139
	y_3 with e VS y_3 without e	0.208	6747.6	0.8353
Manufacturing errors at the one-sigma level	y_1 with e *VS* y_1 without e	0.307	6747.9	0.7581
	y_2 with e VS y_2 without e	24.932	4953.1	<0.001*
	y_3 with e VS y_3 without e	20.158	5003.7	<0.001*

[a] *T-value* is referred to as the T statistic.
*Significant at 0.05 level (two-tailed).

D. CONTROL OF MACHINING PRECISION

The manufacturing error at the three-sigma level is a common control of machining precision, but it only has a subtle impact on performance. To analyze the causes, machining precision is reset at the one-sigma level, and the statistical analysis is rerun. The influence of manufacturing errors on the surface texture performance are compared with both the three-sigma level as well as with the one-sigma level. The differences between y_1, y_2, y_3 with manufacturing errors and y_1, y_2, y_3 without manufacturing errors are shown in Table 4. The results show that the differences in the three-sigma level are not significant, which means that the improvement of surface texture performance is not noticeable. However, the differences between performance with e and without e are significant when the manufacturing errors are at the one-sigma level. As shown in Fig. 10, when the laser texturing only reaches one-sigma performance level, the value of load-carrying capacity decreases, and the value of friction coefficient increases dramatically, which means that the textured performance significantly declines. Therefore, the control of machining precision at the one-sigma level is insufficient. Machining precision should be controlled at the three-sigma level to maintain the texture performance.

Further insight can be gained by performing an in-depth analysis of the influence of each kind of manufacturing errors. For this purpose, two errors are controlled when one error is tested in the condition of the three-sigma level. It is found that more than half of resulting errors contribute to a significant change in surface performance. For example, when d_0 and S_p are fixed at 100 μm and 30% respectively, the manufacturing error of h_g around 1 μm and 5.5 μm results in a dramatic change in friction force ($t = 2.904$, $p = 0.004$; $t = 3.510$, $p < 0.001$). But at approximately 10 μm, no obvious change is apparent ($t = 1.006$, $p = 0.316$). However, all kinds of manufacturing errors in a real manufacturing environment are likely to occur simultaneously, so the mixed effect could be more meaningful.

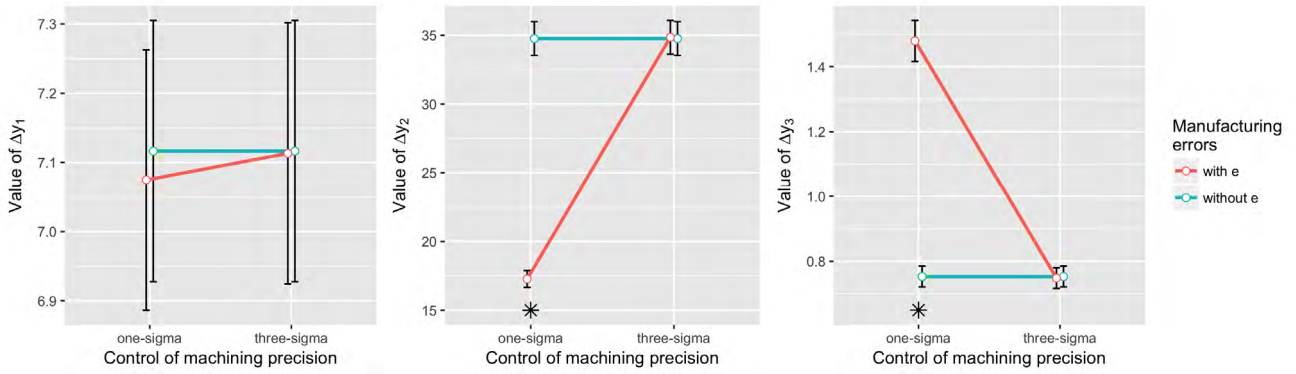

FIGURE 10. Comparisons between performances with one-sigma and three-sigma manufacturing errors (*the difference is significant).

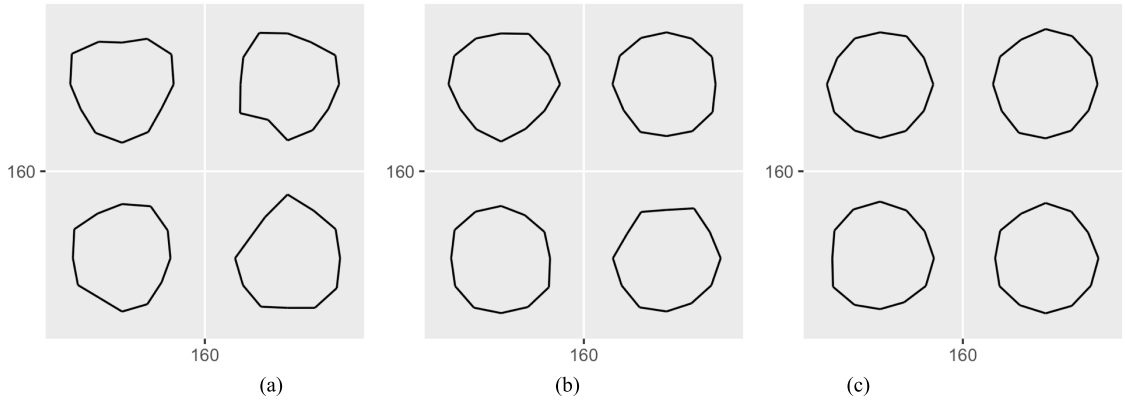

FIGURE 11. The imperfect texture shape controlled by machining precision at the one-sigma level (a), the two-sigma level (b), and the three-sigma level(c).

E. IN-DEPTH ANALYSIS ON IMPERFECT TEXTURE SHAPE

Among those manufacturing errors, imperfect texture shape caused by the dimple diameter's errors is a very difficult problem to tackled using traditional simulation methods. To further analyze its impact on the texture performance, the texture shape with different machining precision is investigated. The area density and the dimple's depth are fixed at 30% and 5.5 μm respectively, and their manufacturing errors are ignored. The dimple's diameter is set as 100 μm. As shown in Fig. 11, texture shape at the one-sigma level is obviously irregular compared to that at the two-sigma level and the three-sigma level. With the increase of machining precision, the average diameter is nearly unchanged, but the variance of diameter is decreased (SD of the diameter, one-sigma level: 9.804; two-sigma level: 5.119; three-sigma level: 3.258) and the texture shape become rounder (roundness of the diameter, one-sigma level: 32.994; two-sigma level: 17.015; three-sigma level: 10.678). Fig. 11 shows that the numerical simulations can generally capture the imperfect texture shape.

The influence of an imperfect texture shape at one-sigma, two-sigma, and three-sigma machining precision on surface texture performance is calculated using the models with BP neural network (as shown in Fig. 12). With the increase of machining precision, variations of the friction force, the load-carrying capacity, and the friction coefficient are decreased. All of them are positive value, which means that the imperfect texture shape improves the performance of friction but decreases the performance of carrying capacity. For the load-carrying capacity, it seems that the performance among different machining precision is not remarkable according to the similar values of the three levels and the large error bars. However, for the friction force, the performance dramatically decreases at the two-sigma level and the three-sigma level. The texture shape should be controlled at least the two-sigma level and preferably at the three-sigma level to gain better performance in terms of friction coefficient.

F. PRACTICAL IMPLICATIONS

The control of texture shape and geometry dimensions can be undemanding once it reaches three-sigma level. Although certain novel texture shapes (e.g., chevron-shape) have significantly higher surface performance than circular textures [5], the circular dimple is still commonly used in LST. However, the dimple shape is not easily to be manufactured as a perfect shape, such as perfect circle, because

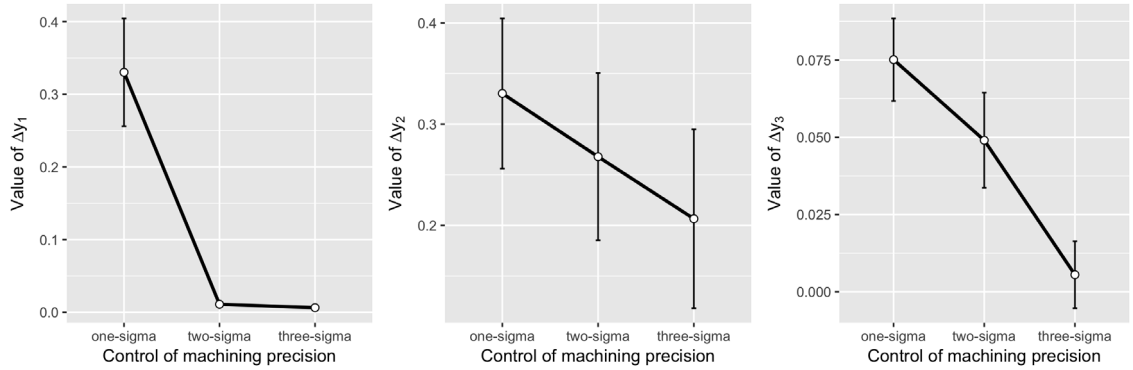

FIGURE 12. The influence of imperfect texture shape with different machining precision on the performance.

the manufacturing errors of dimple diameters probably have impact on the dimple shape. It is found that the flaw in texture shape and manufacturing errors of geometry dimension do not have adverse impact on performance at the three-sigma level. In contrast, the imperfect texture shape and dimension uncertainly at the one-sigma level can dispel the texture's positive effects.

In addition, to better represent the LST dimples generated by high pulses as shown in Fig. 2, the imperfect texture shape needs to be divided into more sections. According to recent research, very short pulses (e.g., from femtosecond lasers) are used in LST to prevent the problem of lateral rims and surface roughness. Lateral rims around the dimple edge is a serious problem because they are hard to remove. In order to increase the performance, Amanov *et al.* [15] combined laser micropolishing and laser ablation for surface texturing to smooth the ablated dimple bottom surface consistently, and Perry *et al.* [22], [23] reduced the average surface roughness of 5 μm wavelength line features from 0.112 μm to 0.015 μm. However, this is time-consuming and expensive for reprocessing the semifinished product since laser surface texturing process is already finished. Their studies focused on improving roughness of dimple bottom surface, which means that the benefit of their studies probably is more remarkable for shallow dimples. In terms of sufficiently deep dimples, the dimple bottom roughness have a relatively little effect [15], and the roughness of dimple edge and broadside may have more effect. Adopting the pulsed laser micropolishing to reduce roughness should be further considered in practical implications, and the numerical experiment and statistical analysis in this research might provide an approach to estimate the roughness.

Another important factor is the implementation of the mass-conservative algorithm to model the cavitation effect within the dimples. Cavitation in dimples is shown to have significant influence on the performance of near-parallel textured contacts [24]. Using the Jakobsson–Floberg–Olsson (JFO) model and its modifications which are widely used cavitation model can conserve mass continuity and improve numerical instability, but it increases the model complexity [25]–[28]. In view of cavitation effects and the real environment, surface texture performance might have other variations, thus implementing real experiment to validate the results may be necessary.

In general, to enhance the texture performance, practitioners should first know the most important performance parameter and then determine the value of the dimple diameter, the area density, and the dimple depth according to the primary stage of the research [19]. The control of manufacturing errors from laser texturing at three-sigma performance level is adequate, and the machining precision of one sigma is not recommended.

V. CONCLUSIONS

This research explores the performance of surface textures with imperfect texture shape and dimensional uncertainty based on statistical models. A general method for quantifying uncertainty of texture shape and dimensions is developed. There are three major findings in this research:

First, the models with back propagation neural network and genetic algorithm can explain and predict the performance of surface textures with imperfect texture shape and dimensional uncertainty. The models could explain 99.73%, 97.51%, and 96.52% of variations in the friction force, the load-carrying capacity, and the coefficient of friction, respectively.

Second, the statistical models reveal that the most influential factor of the friction force is the manufacturing errors of area density. For the load-carrying capacity and the coefficient of friction, the most influential uncertainty is manufacturing errors associated with the dimple diameter, resulting in imperfect shapes.

Third, manufacturing errors at the three-sigma level slightly increase the performance of surface textures about 0.5% on average, which is not significant. However, the laser texturing that reaches one-sigma performance level can dramatically reduce the load-carrying capacity and increase the coefficient of friction. Specifically, when other dimensions are set as 30% for the area density, 5.5 μm for the dimple's depth, and 100 μm for the dimple's diameter, the imperfect texture shape at the three-sigma level

can yield better performance than lower levels of control of machining precision. In order to obtain the optimized value of surface texture performance, manufacturing errors at the one-sigma level should be avoided.

REFERENCES

[1] H. Costa and I. M. Hutchings, "Some innovative surface texturing techniques for tribological purposes," *Proc. Inst. Mech. Eng., J, J. Eng. Tribol.*, vol. 229, pp. 429–448, Jun. 2014.
[2] C. Vincent, G. Monteil, T. Barriere, and J. C. Gelin, "Control of the quality of laser surface texturing," *Microsyst. Technol.*, vol. 14, pp. 1553–1557, Oct. 2008.
[3] R. B. Siripuram, "Analysis of hydrodynamic effects of microasperity shapes on thrust bearing surfaces," M.S. thesis, Dept. Mech. Eng., Univ. Kentucky, Lexington, KY, USA, 2003.
[4] M. Qiu, A. Delic, and B. Raeymaekers, "The effect of texture shape on the load-carrying capacity of gas-lubricated parallel slider bearings," *Tribol. Lett.*, vol. 48, no. 3, pp. 315–327, 2012.
[5] C. Shen and M. M. Khonsari, "Texture shape optimization for seal-like parallel surfaces: Theory and experiment," *Tribol. Trans.*, vol. 59, no. 4, pp. 698–706, 2016.
[6] T. Nanbu, N. Ren, Y. Yasuda, D. Zhu, and Q. J. Wang, "Micro-textures in concentrated conformal-contact lubrication: Effects of texture bottom shape and surface relative motion," *Tribol. Lett.*, vol. 29, no. 8, pp. 241–252, 2008.
[7] D. Gropper, L. Wang, and T. J. Harvey, "Hydrodynamic lubrication of textured surfaces: A review of modeling techniques and key findings," *Tribol. Int.*, vol. 94, pp. 509–529, Feb. 2016.
[8] X. Wang, J. Wang, B. Zhang, and W. Huang, "Design principles for the area density of dimple patterns," *Proc. Inst. Mech. Eng., J, J. Eng. Tribol.*, vol. 229, pp. 538–546, May 2014.
[9] L. Galda, P. Pawlus, and J. Sep, "Dimples shape and distribution effect on characteristics of Stribeck curve," *Tribol. Int.*, vol. 42, no. 10, pp. 1505–1512, 2009.
[10] T. Ibatan, M. Uddin, and M. Chowdhury, "Recent development on surface texturing in enhancing tribological performance of bearing sliders," *Surf. Coatings Technol.*, vol. 272, pp. 102–120, Jun. 2015.
[11] D. Yan, N. Qu, H. Li, and X. Wang, "Significance of dimple parameters on the friction of sliding surfaces investigated by orthogonal experiments," *Tribol. Trans.*, vol. 53, no. 5, pp. 703–712, 2010.
[12] D. G. Coblas, A. Fatu, A. Maoui, and M. Hajjam, "Manufacturing textured surfaces: State of art and recent developments," *Proc. Inst. Mech. Eng., J, J. Eng. Tribol.*, vol. 229, pp. 3–29, Jul. 2015.
[13] U. Sudeep, N. Tandon, and R. K. Pandey, "Performance of lubricated rolling/sliding concentrated contacts with surface textures: A review," *J. Tribol.*, vol. 137, no. 3, p. 031501, 2015.
[14] Y. Gao, B. Wu, Y. Zhou, and S. Tao, "A two-step nanosecond laser surface texturing process with smooth surface finish," *Appl. Surf. Sci.*, vol. 257, no. 23, pp. 9960–9967, 2011.
[15] A. Amanov, R. Tsuboi, H. Oe, and S. Sasaki, "The influence of bulges produced by laser surface texturing on the sliding friction and wear behavior," *Tribol. Int.*, vol. 60, pp. 216–223, Apr. 2013.
[16] K. Simunovic, G. Simunovic, and T. Saric, "Predicting the surface quality of face milled aluminium alloy using a multiple regression model and numerical optimization," *Meas. Sci. Rev.*, vol. 13, pp. 265–272, 2013.
[17] F. Puh, Z. Jurkovic, M. Perinic, M. Brezocnik, and S. Buljan, "Optimization of machining parameters for turning operation with multiple quality characteristics using Grey relational analysis," *Tehn. kivjesnik*, vol. 23, no. 2, pp. 377–382, 2016.
[18] B. S. Prasad and M. P. Babu, "Correlation between vibration amplitude and tool wear in turning: Numerical and experimental analysis," *Eng. Sci. Technol., Int. J.*, vol. 20, no. 1, pp. 197–211, 2016.
[19] F. Mo, C. Shen, J. Zhou, and M. M. Khonsari, "Statistical analysis of surface texture performance with provisions with uncertainty in texture dimensions," *IEEE Access*, vol. 5, pp. 5388–5398, 2017.
[20] S. C. Shen and M. M. Khonsari, "Numerical optimization of texture shape for parallel surfaces under unidirectional and bidirectional sliding," *Tribol. Int.*, vol. 82, pp. 1–11, Feb. 2015.
[21] Y. Xiang, S. Gubian, B. Suomela, and J. Hoeng, "Generalized simulated annealing for global optimization: The GenSA package," *R J.*, vol. 5, pp. 13–28, Jun. 2013.
[22] T. L. Perry, D. Werschmoeller, N. A. Duffie, X. Li, and F. E. Pfefferkorn, "Examination of selective pulsed laser micropolishing on microfabricated nickel samples using spatial frequency analysis," *J. Manuf. Sci. Eng.*, vol. 131, p. 021002, Feb. 2009.
[23] T. L. Perry, D. Werschmoeller, X. Li, F. E. Pfefferkorn, and N. A. Duffie, "The effect of laser pulse duration and feed rate on pulsed laser polishing of microfabricated nickel samples," *J. Manuf. Sci. Eng.*, vol. 131, p. 031002, Apr. 2009.
[24] M. Dobrica, M. Fillon, M. Pascovici, and T. Cicone, "Optimizing surface texture for hydrodynamic lubricated contacts using a mass-conserving numerical approach," *Proc. Inst. Mech. Eng., J, J. Eng. Tribol.*, vol. 224, pp. 737–750, Jun. 2010.
[25] J. Zhang and Y. Meng, "Direct observation of cavitation phenomenon and hydrodynamic lubrication analysis of textured surfaces," *Tribol. Lett.*, vol. 46, no. 2, pp. 147–158, 2012.
[26] Y. Qiu and M. M. Khonsari, "On the prediction of cavitation in dimples using a mass-conservative algorithm," *J. Tribol.*, vol. 131, no. 4, p. 041702, 2009.
[27] C. Shen and M. M. Khonsari, "On the magnitude of cavitation pressure of steady-state lubrication," *Tribology Lett.*, vol. 51, no. 1, pp. 153–160, 2013.
[28] M. Fesanghary and M. M. Khonsari, "A modification of the switch function in the Elrod cavitation algorithm," *J. Tribol.*, vol. 133, no. 2, p. 024501, 2011.

FAN MO received the B.S. degree in industrial engineering from Chongqing University, Chongqing, China, in 2015, where he is currently pursuing the M.S. degree in management science and engineering.

He is the author or co-author of nine research publications, including seven journal papers. His research interest includes applied statistical analysis, human–computer interaction, interface design for mobile and wearable devices, and social network analysis.

CONG SHEN received the Ph.D. degree in mechanical engineering from Louisiana State University, Baton Rouge, LA, USA, in 2016.

He is the author or co-author of several research publications. His research interest includes tribology, machinery performance analysis, and numerical analysis.

JIA ZHOU received the B.S. degree in industrial engineering from Tongji University, Shanghai, China, in 2007, and the Ph.D. degree from the Institute of Human Factors and Ergonomics, Tsinghua University, Beijing, China, in 2013.

From 2011 to 2012, she was a Visiting Scholar with the Trace Research and Development Center, University of Wisconsin-Madison, Madison, WI, USA. Since 2013, she has been an Assistant Professor with the Department of Industrial Engineering, Chongqing University, Chongqing, China. She is the author or co-author of more than 40 research publications, including 23 journal papers. Her main research deals with applied statistical analysis, human–computer interaction, universal design, technology acceptance, usability engineering, mobile computing, and accessibility.

Dr. Zhou was offered an appointment as an Honorary Associate with the Trace Research and Development Center for her contributions to the research project. She is the Co-Chair of the International Conference on Human Aspects of IT for the Aged Population, and on the editorial board of *International Journal of Human-Computer Interaction*, *Behaviour and Information Technology*, and *Universal Access in the Information Society*.

MICHAEL M. KHONSARI received the B.S., M.S., and Ph.D. degrees in mechanical engineering from The University of Texas at Austin, Austin, TX, USA.

From 1984 to 1988, he was a Professor with The Ohio State University, Columbus, OH, USA. Prior to joining Louisiana State University, Baton Rouge, LA, USA, he spent a number of years as a Faculty Member with The Ohio State University, University of Pittsburgh, and served as the Chairman of the Department of Mechanical Engineering and Energy Processes with Southern Illinois University. He is a Dow Chemical Endowed Chair and a Professor and the Director of the Center for Rotating Machinery with the Department of Mechanical Engineering, Louisiana State University. He is the author of several books. His research interests include tribology (friction, lubrication, and wear), machinery performance analysis, numerical analysis, and heat transfer. He is known for his research in tribology and, in particular, the application of thermodynamic methods in tribology.

Prof. Khonsari is a fellow of the ASME. He received the ASME Mayo Hersey and Burt L. Newkirk Awards, the STLE Presidential Award, the Alcoa Foundation Award, and the William Kepler Whiteford Faculty Fellow Award from the University of Pittsburgh. He has also served as a Research Faculty Fellow with the NASA Lewis (currently Glenn) Research Center, Wright-Patterson Air Force Laboratories, and the U.S. Department of Energy.